CHEMISTRY
A European Journal

Supporting Information

Desymmetrization of an Octahedral Coordination Complex Inside a Self-Assembled Exoskeleton

Mark D. Johnstone,[a, b, c] Eike K. Schwarze,[b] Jennifer Ahrens,[d] Dirk Schwarzer,[d] Julian J. Holstein,[c] Birger Dittrich,[e] Frederick M. Pfeffer,*[a] and Guido H. Clever*[b, c]

chem_201602497_sm_miscellaneous_information.pdf

Contents

Experimental Procedures and Characterisation Data

All reagents were obtained commercially and used without purification unless indicated otherwise. DMAD was distilled prior to use using a Kugelrohr short-path vacuum distillation apparatus (70–80 °C, 5 mbar).

NMR experiments were performed on a JEOL JNM-Ex 270 MHz, Eclipse JNM-ECP 400 MHz FT-NMR, Bruker AVANCE III 300 MHz, or a Bruker AVANCE III 500 MHz FT-NMR spectrometer. Samples were dissolved in $CDCl_3$, DMSO-d_6, CD_3CN, CD_3OD or CD_2Cl_2. ^1H NMR spectra are reported as chemical shift (ppm) (multiplicity (s = singlet, d = doublet, t = triplet, m= multiplet, br = broadened), *J* coupling (Hz), integral, assignment).

High-resolution mass spectral data was collected on either an Agilent Technologies LC/MSD TOF or a Bruker Apex IV ESI-FTICR Mass Spectrometer or a LC Agilent 1200 MS 6520 QTOF with dual electrospray ionisation source. Samples were dissolved in MeOH or CH_3CN at a concentration of less than 0.1 mg/mL.

Thin layer chromatography was performed on Merck TLC silica gel 60 F_{254} plates, and visualised using UV light (λ = 254 nm and 365 nm) and a potassium permanganate oxidising dip ($KMnO_4$, H_2O, K_2CO_3). Column chromatography was performed using silica gel 60 (230–400 mesh).

All microwave reactions were closed vessel reactions performed using a CEM Discover S-class microwave reactor.

Melting points were obtained using a Stuart SMP30 melting point apparatus.

Compounds were named according to the IUPAC guidelines following the von Baeyer system for polycyclic compounds.[1] The relative stereodescriptors α/β are used to describe the configuration of the substituents on the ring system.

All Pd-coordination experiments were performed in deuterated acetonitrile with a ligand concentration of 2.8 mM. A $[Pd(CH_3CN)_4](BF_4)_2$ stock solution of 15 mM concentration was used to introduce the metal. After addition of 0.5 equiv. Pd-solution (with respect to the ligand) the samples were heated to 70 °C without stirring for 12–16 h and subjected to NMR spectroscopic and ESI mass spectrometric characterisation without further workup or purifications steps.

***N*-(4-Methoxyphenylmethyl)phthalimide**[2]

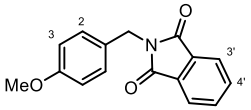

Freshly prepared potassium phthalimide (1.63 g, 8.80 mmol), 4-methoxybenzylchloride (1.0 mL, 7.34 mmol) and DMF (4 mL) were added to a flask and refluxed for 18 h. After cooling the contents were poured onto H_2O (20 mL), the white precipitate was collected by vacuum filtration, washed with H_2O (3 × 5 mL) and then dried affording a white solid (1.96 g, 99%).

^{1}H NMR (270 MHz, $CDCl_3$) δ 7.82 (q, *J* = 3.0 Hz, 2H, $H_{3'}$), 7.67 (q, *J* = 3.0 Hz, 2H, $H_{4'}$), 7.37 (d, *J* = 8.7 Hz, 2H, $H_{2,6}$), 6.82 (d, *J* = 8.7 Hz, 2H, $H_{3,5}$), 4.77 (s, 2H, CH_2), 3.75 (s, 3H, Me).

^{13}C NMR (68 MHz, $CDCl_3$) δ 168.2, 159.3, 134.0. 132.3, 130.2, 128.7, 123.4, 114.1, 55.4, 41.1.

HRMS (ESI-TOF) *m/z*: $[M + Na]^+$ Calcd for $C_{16}H_{14}NO_3Na$ 290.0788, found 290.0799.

mp 127–129 °C (lit.[2] mp 132 °C)

4-Methoxybenzylamine[2]

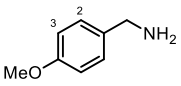

Hydrazine hydrate (95 µL, 2.00 mmol) was added to a solution of *N*-(4-methoxyphenylmethyl)phthalimide (103 mg, 0.39 mmol) in THF (5 mL) and the reaction was refluxed for 16 h. A white precipitate was observed within 1 h of heating. After completion (TLC, R_f = 0.46 in 9:1:0.01 CH_2Cl_2/MeOH/NH_4OH) the solvent was removed *in vacuo* and the reaction contents were partitioned between CH_2Cl_2 (15 mL) and 2 M NaOH (15 mL). The organic phase was separated, dried ($MgSO_4$), filtered and the solvent evaporated to give a clear oil (54 mg, 99%).

^{1}H NMR (270 MHz, $CDCl_3$) δ 7.20 (d, *J* = 8.7 Hz, 2H, $H_{2,6}$), 6.85 (d, *J* = 8.7 Hz, 2H, $H_{3,5}$), 3.78 (s, 5H, CH_2, Me), 1.47 (br s, 2H, NH_2).

^{13}C NMR (68 MHz, $CDCl_3$) δ 158.6, 135.6, 128.3, 114.0, 55.4, 46.0.

***R*$_f$** = 0.46 in CH_2Cl_2/MeOH/NH_4OH (9:1:0.01)

(6α,9α,10α,11α,12α,15α)-3-(4-Methoxybenzyl)-3-azahexacyclo[7.6.0.0^{1,5}.0^{5,12}.0^{6,10}.0^{11,15}]pentadeca-7,13-diene-2,4-dione

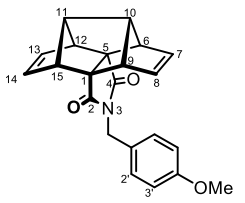

(6α,9α,10α,11α,12α,15α)-3-Oxahexacyclo[7.6.0.0^{1,5}.0^{5,12}.0^{6,10}.0^{11,15}]pentadeca-7,13-diene-2,4-dione[3] (81 mg, 0.358 mmol) was dissolved in CH_2Cl_2 (2 mL) before 4-methoxybenzylamine (49 mg, 0.358 mmol) was added. After refluxing for 1 h the solvent was removed by reduced pressure and Ac_2O (1.5 mL) was added and the reaction mixture was heated at 80 °C for 16 h. After this time the volatiles were removed *in vacuo* and chromatographic purification (1:5 EtOAc/petroleum ether) afforded the desired product (87 mg, 70%).

^{1}H NMR (270 MHz, $CDCl_3$) δ 7.17 (d, *J* = 8.9 Hz, 2H, $H_{2'}$), 6.75 (d, *J* = 8.9 Hz, 2H $H_{3'}$), 5.92 (t, *J* = 1.9 Hz, 4H, $H_{7,8,13,14}$), 4.44 (s, 2H, CH_2Ar), 3.74 (s, 3H, Me), 3.43 (dt, *J* = 2.5, 2.0 Hz, 4H, $H_{6,9,12,15}$), 2.84 (dd, *J* = 3.1, 1.3 Hz, 2H, $H_{10,11}$).

^{13}C NMR (68 MHz, $CDCl_3$) δ 175.2, 158.9, 132.2, 129.4, 128.8, 113.7, 66.9, 64.4, 62.3, 55.3, 41.5.

HRMS (ESI-TOF) *m/z*: $[M + H]^+$ Calcd for $C_{22}H_{20}O_3N$ 346.1438, found 346.1433.

mp 169–171 °C

***R*$_f$** = 0.45 in EtOAc/petroleum ether (1:5)

(6α,9α,10α,11α,12α,15α)-3-Azahexacyclo[7.6.0.0^{1,5}.0^{5,12}.0^{6,10}.0^{11,15}]pentadeca-7,13-diene-2,4-dione[4]

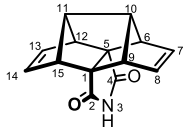

Method A

A solution of the PMB-imide (46 mg, 0.13 mmol) in CH_3CN/H_2O (5:1, 5 mL) was cooled to 0 °C before ceric ammonium nitrate (730 mg, 1.33 mmol) was added in a single portion. The reaction mixture was allowed to warm to ambient temperature and stirred for 16 h. Following this time, sat. $NaHCO_3$ (10 mL) was added and the resulting mixture was transferred to a separatory funnel and extracted with CH_2Cl_2 (3 × 5 mL). The organic phase was washed with brine (10 mL), dried, and concentrated to dryness. The resulting material was added to a mixture of MeOH (5 mL) and 2 M KOH (5 mL) which was heated at 50 °C for 1 h. Following this time the reaction mixture was neutralised with 2 M HCl and extracted with CH_2Cl_2 (3 × 5 mL). The combined organic phase was dried and concentrated to give imide **1** (21 mg, 70%).

Method B

(6α,9α,10α,11α,12α,15α)-3-Oxahexacyclo[7.6.0.0^{1,5}.0^{5,12}.0^{6,10}.0^{11,15}]pentadeca-7,13-diene-2,4-dione[3] (11 mg, 0.049 mmol), ammonium acetate (200 mg) and AcOH (1 mL) were sealed in a microwave vial and heated using microwave irradiation at 140 °C for 10 min. The contents were poured onto H_2O (20 mL) and extracted with CH_2Cl_2 (3 × 5 mL) then the organics were dried and evaporated. The resulting residue was passed through a short silica plug with EtOAc as the eluent to give the desired imide (6 mg, 50%).

^{1}H NMR (270 MHz, $CDCl_3$) δ 7.63 (br s, 1H, NH), 6.07 (t, *J* = 1.9 Hz, 4H, $H_{7,8,13,14}$), 3.45 (dd, *J* = 4.2, 2.2 Hz, 4H, , $H_{6,9,12,15}$), 2.87 (t, *J* = 1.7 Hz, 2H, $H_{10,11}$).

^{13}C NMR (68 MHz, $CDCl_3$) δ 175.3, 132.3, 68.4, 64.5, 62.5.

HRMS (ESI-TOF) *m/z*: $[M + H]^+$ Calcd for $C_{14}H_{12}NO_2$ 226.0863, found 226.0853.

mp >200 °C dec (lit.[5] mp 245 °C dec)

***R*$_f$** = 0.67 in EtOAc

Tetramethyl (1α,2β,3α,9α,10β,11α,12β,13α,14α,18α,19α,20β,21α,22β,23α,24α,25α,26α,27β,28α,29β,30α,31α,35α,36α,37β)-5,7,15,17,32,34-hexaoxo-16,33-bis(pyridin-4-yl)-38,40-dioxa-6,16,33-triazahexadecacyclo[26.9.1.1^{11,21}.1^{13,19}.1^{30,36}.0^{2,27}.0^{3,25}.0^{4,8}.0^{4,23}.0^{8,26}.0^{9,24}.0^{10,22}.0^{12,20}.0^{14,18}.0^{29,37}.0^{31,35}]hentetraconta-1,11,21,28-tetracarboxylate

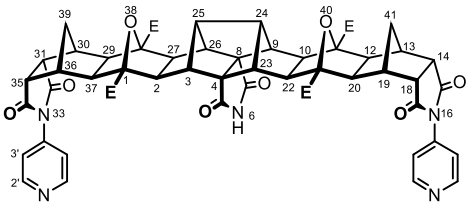

Alkene **1** (8.1 mg, 0.036 mmol), epoxide **2** (28.6 mg, 0.072 mmol) and DMF (1.5 mL) were sealed in a 10 mL microwave vial and heated by microwave irradiation to 150 °C for 10 min. After the reaction had cooled the solvent was removed *in vacuo* and the resulting solids were column purified (5% MeOH in CH_2Cl_2, R_f = 0.30) to give **L** as a white powder (16 mg, 44%).

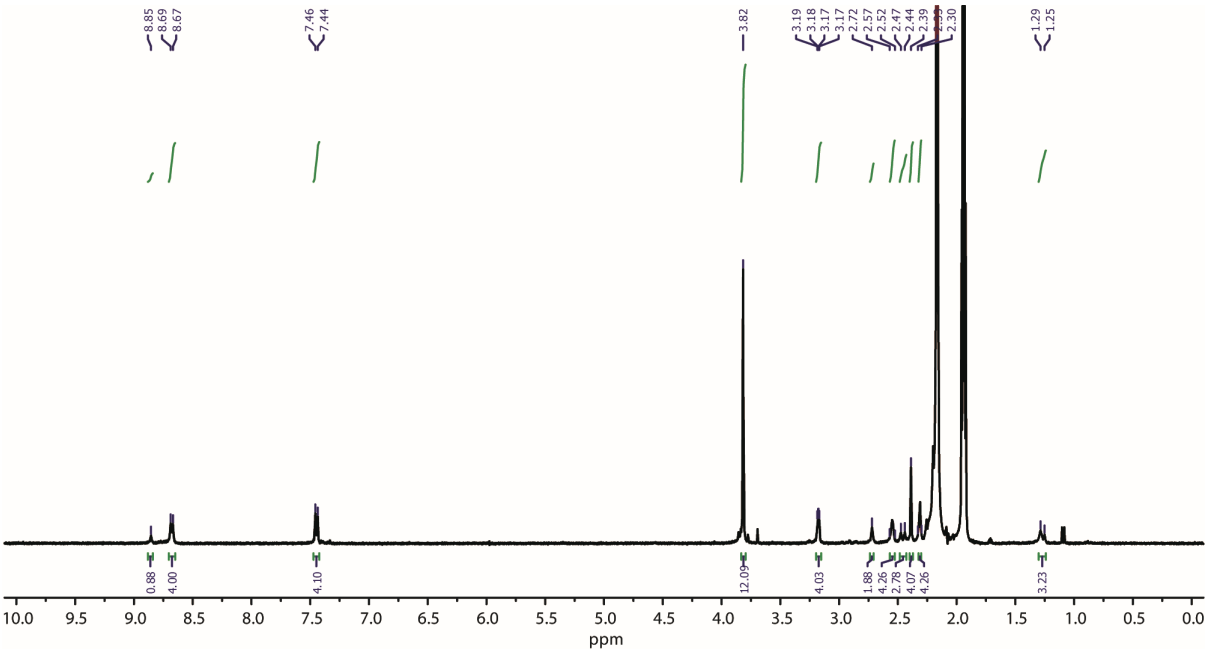

^{1}H NMR (300 MHz, CD_3CN) δ 8.85 (s, 1H, NH), 8.68 (d, *J* = 6.3 Hz, 2H, $H_{2'}$), 7.45 (d, *J* = 6.3 Hz, 2H, $H_{3'}$), 3.82 (s, 12H, 4 × Me), 3.18 (dd, *J* = 3.4, 2.0 Hz, 4H, $H_{14,18,31,35}$), 2.72 (br s, 2H, $H_{24,25}$), 2.57–2.52 (m, 4H, $H_{13,19,30,36}$), 2.46 (d, *J* = 10.2 Hz, 2H, $H_{39s,41s}$), 2.39 (s, 4H, $H_{2,10,22,27}$), 2.33–2.30 (m, 4H, $H_{3,9,23,26}$), 1.27 (d, *J* = 10.2 Hz, 2H, $H_{39a,41a}$).

^{13}C NMR (101 MHz, 5% CD_3OD in $CDCl_3$) δ 175.2, 175.0, 167.7, 156.4, 150.0, 120.2, 90.5, 61.4, 55.3, 52.9, 49.5, 48.9, 48.5, 48.1, 41.8, 37.8.

HRMS (ESI-QTOF) *m/z*: $[M + H]^+$ Calcd for $C_{54}H_{48}N_5O_{16}$ 1022.3091, found 1022.3095.

mp >260 °C dec

***R*$_f$** = 0.30 (5% MeOH in CH_2Cl_2)

L + Pd:

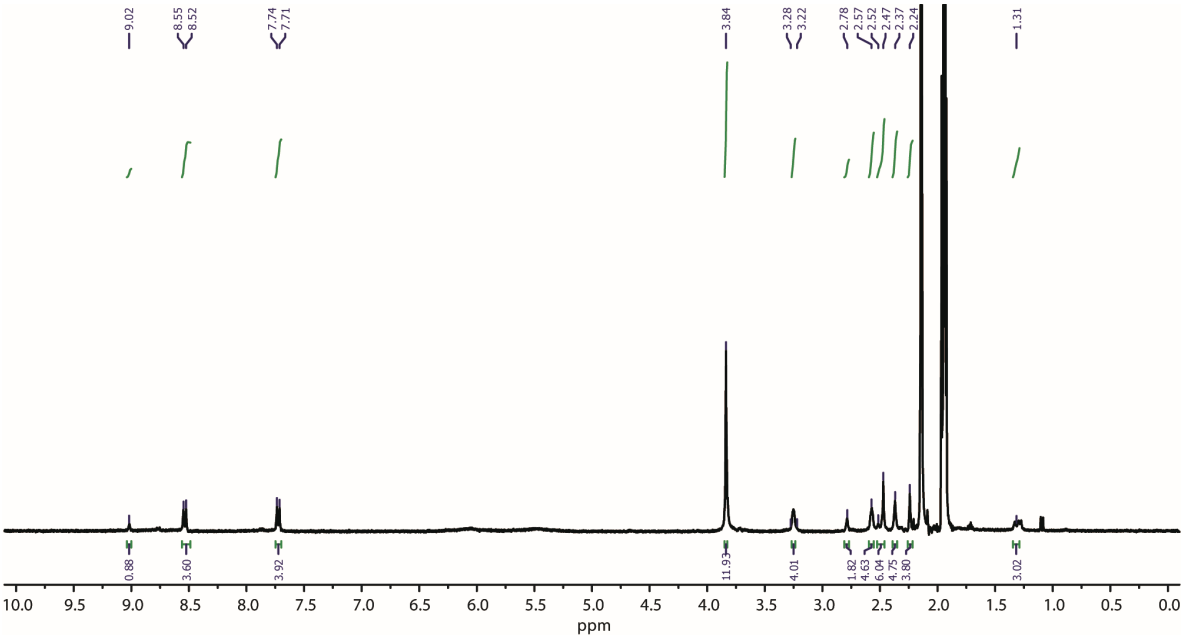

^{1}H NMR (300 MHz, CD_3CN) δ 9.02 (s, 1H, NH), 8.54 (d, *J* = 6.1 Hz, 4H, $H_{2'}$), 7.73 (d, *J* = 6.1 Hz, 2H, $H_{3'}$), 3.84 (s, 12H, 4 × Me), 3.28–3.22 (m, 4H, $H_{14,18,31,35}$), 2.78 (s, 2H, $H_{24,25}$), 2.57 (s, 4H, $H_{13,19,30,36}$), 2.52–2.47 (m, 6H, $H_{39s,41s,2,10,22,27}$), 2.37 (s, 4H, $H_{3,9,23,26}$), 2.24 (s, 4H, $H_{12,20,29,37}$), 1.31 (d, *J* = 10.1 Hz, 2H, $H_{39a,41a}$).

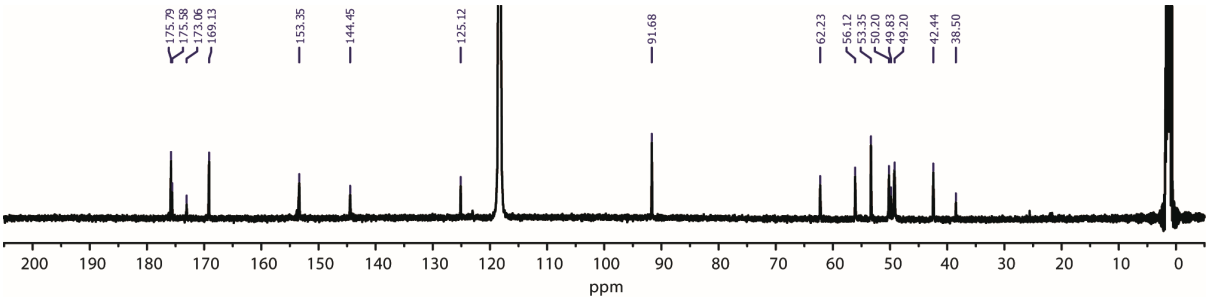

^{13}C NMR (126 MHz, CD_3CN) δ 175.8, 175.6, 173.1, 169.1, 153.4, 144.5, 125.1, 91.7, 62.2, 56.1, 53.4, 50.2, 49.8, 49.2, 42.4, 38.5.

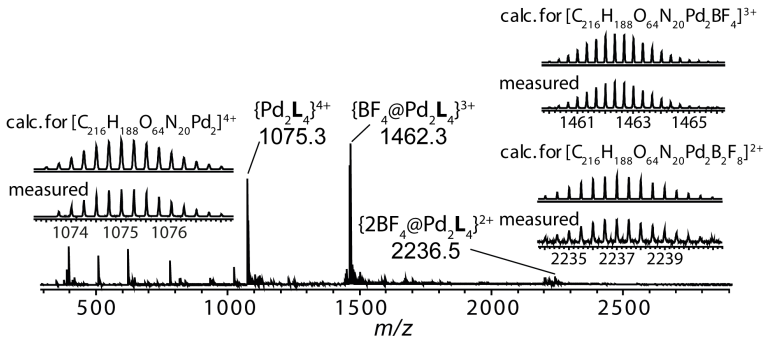

HRMS (ESI-FTICR) *m/z*: calcd. for $[C_{216}H_{188}N_{20}O_{64}Pd_2]^{4+}$ 1075.0052; found 1075.0047; calcd. for $[C_{216}H_{188}N_{20}O_{64}Pd_2BF_4]^{3+}$ 1462.3417; found 1462.3397; calcd. for $[C_{216}H_{188}N_{20}O_{64}Pd_2B_2F_8]^{2+}$ 2237.0147; found 2237.0093.

Molecular Modelling

The computational experiments were performed using IEFPCM solvation model as implemented in Gaussian '09[6]. Energies in the tables are given relative to the structure mentioned in the header.

Table S1: Energy differences between the cage and the butterfly structure based on ligand **L**.

	Relative to butterfly [kJ/mol]
Cage	−477

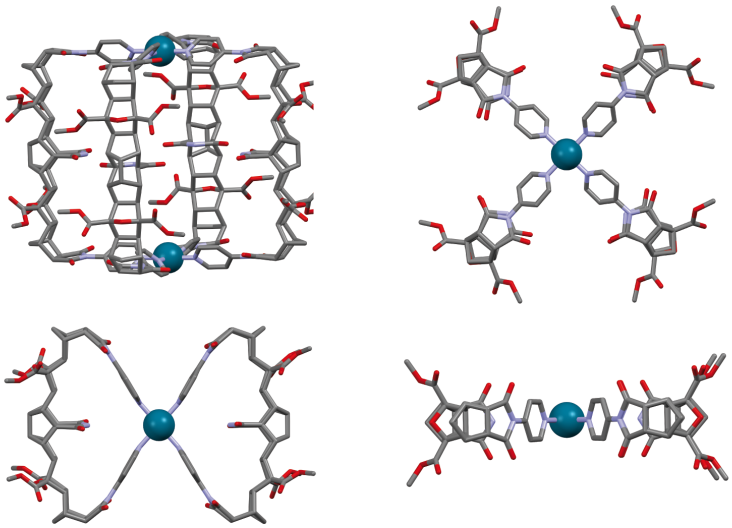

Figure S1: Calculated structures of plausible self-assemblies based on ligand **L** (PM6, solvent = acetonitrile). Top: cage, bottom: butterfly.

The IR spectroscopic region containing the CN stretching vibrations of the tetragonally desymmetrized guest $[Pt(CN)_6]^{2-}$ depicted in Figure 4 of the main text was calculated by fixing an array of NH hydrogen bond donors and two Pd(II) cations (or alternatively Pd(II)(pyridine)$_4$ fragments) around an unconstraint $[Pt(CN)_6]$ complex. Angular constraints were applied to the Pt centre to prevent the guest from escaping the Pd(II)/hydrogen-donor environment but no restrictions were forced upon the Pt-C or C-N bond lengths or angles. Distances of the surrounding fragments were adopted from the X-ray analysis (corrected for slight deformations due to packing effects). The system was geometry optimized on the DFT ωB97XD/def2SVP level of theory using Gaussian '09[6] and the IR active vibrations were extracted from the frequency calculation and scaled by a factor of 0.95 (as suggested for the used functional on http://t1.chem.umn.edu/freqscale/index.html)

^{1}H NMR Spectroscopy Titrations

General procedure

All ^{1}H NMR titrations were performed using 500 µL of {Pd_2**L**$_4$} solution in in CD_3CN with an initial concentration of 0.7 mM. Guest solutions (as tetrabutylammonium salts).were prepared with concentrations of 15 mM in CD_3CN). The chemical shift of the N–H proton was recorded following each addition of the guest to the {Pd_2**L**$_4$} cage.

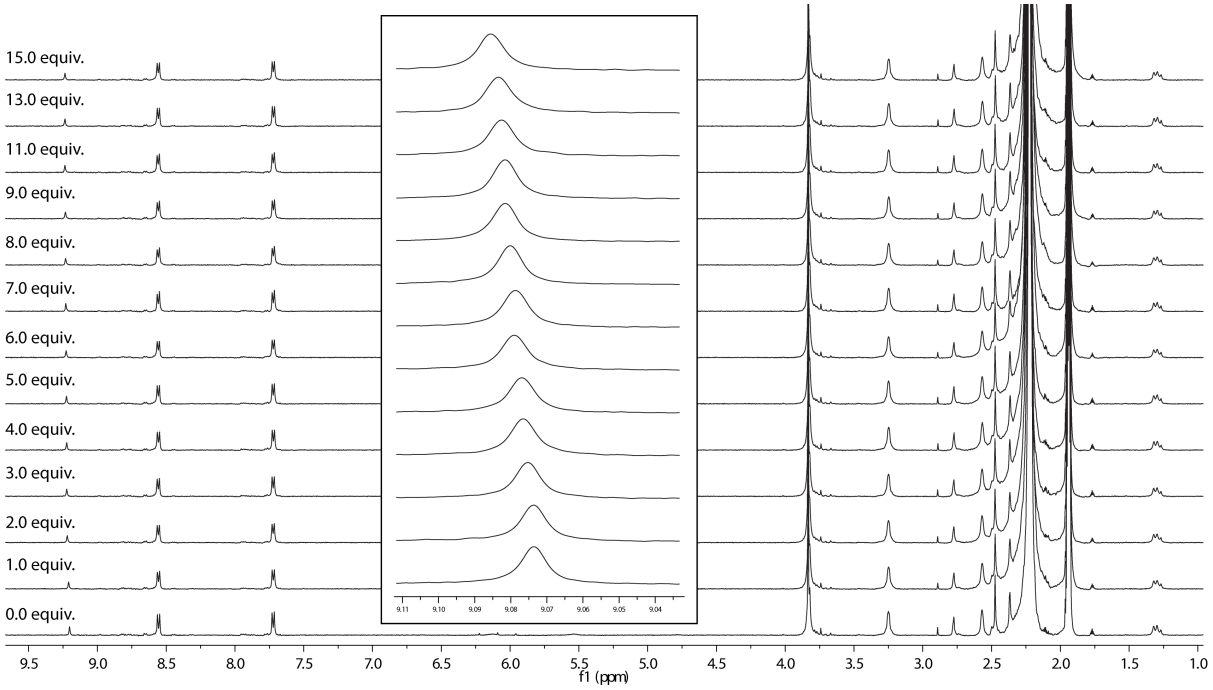

Figure S2 ^{1}H NMR titration (400 MHz, 298 K, CD_3CN) of {Pd_2**L**$_4$} with [$Cr(CO)_6$].

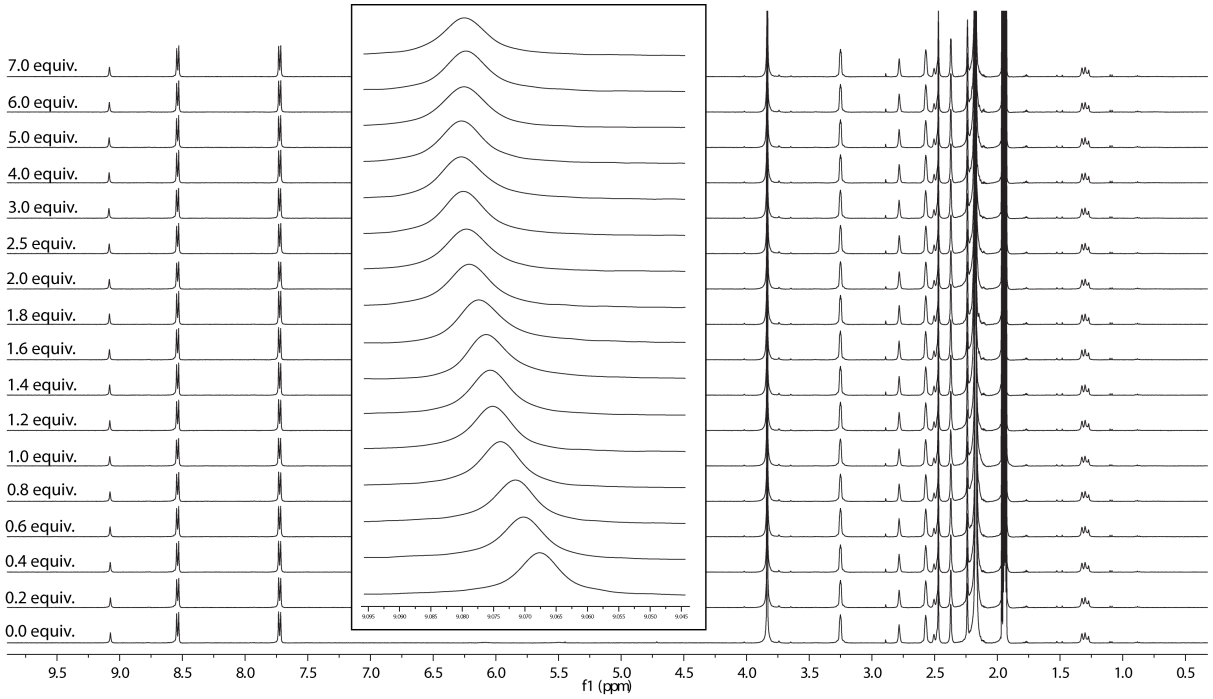

Figure S3 ^{1}H NMR titration (400 MHz, 298 K, CD_3CN) of {Pd_2**L**$_4$} with [$W(CO)_6$].

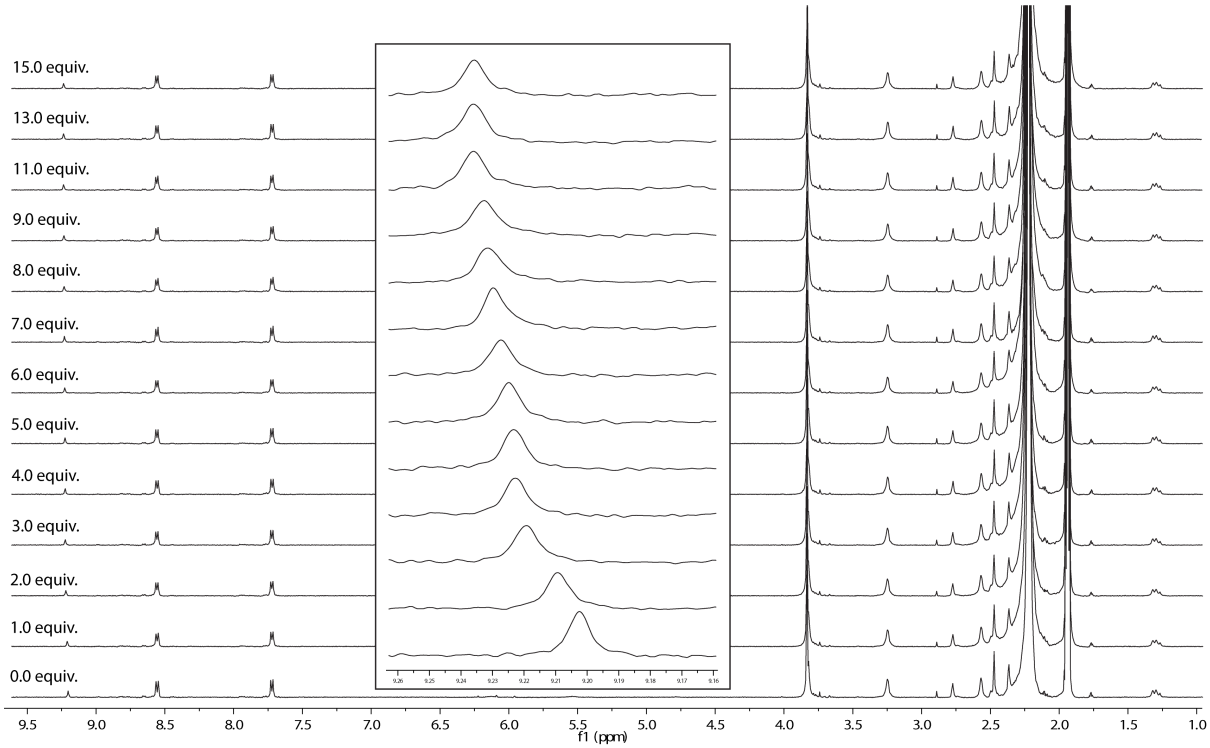

Figure S4 ^{1}H NMR titration (400 MHz, 298 K, CD_3CN) of $\{Pd_2\mathbf{L}_4\}$ with $[Mo(CO)_6]$.

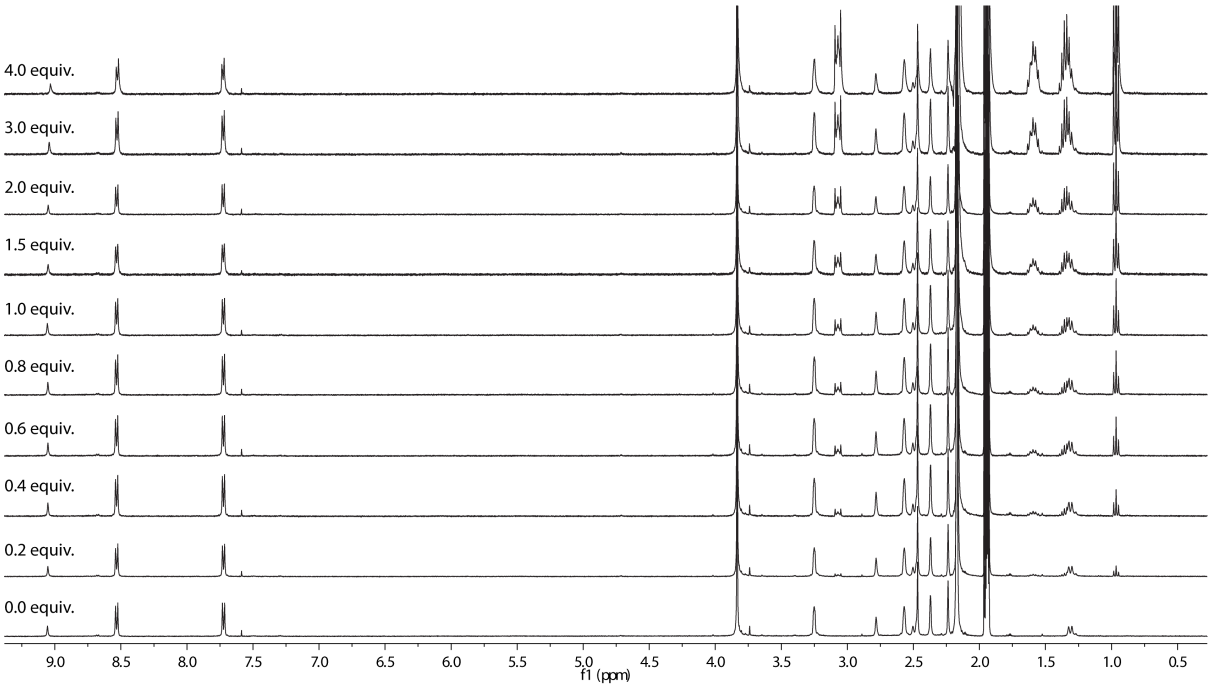

Figure S5 ^{1}H NMR titration (400 MHz, 298 K, CD_3CN) of $\{Pd_2\mathbf{L}_4\}$ with $(Bu_4N)[PF_6]$.

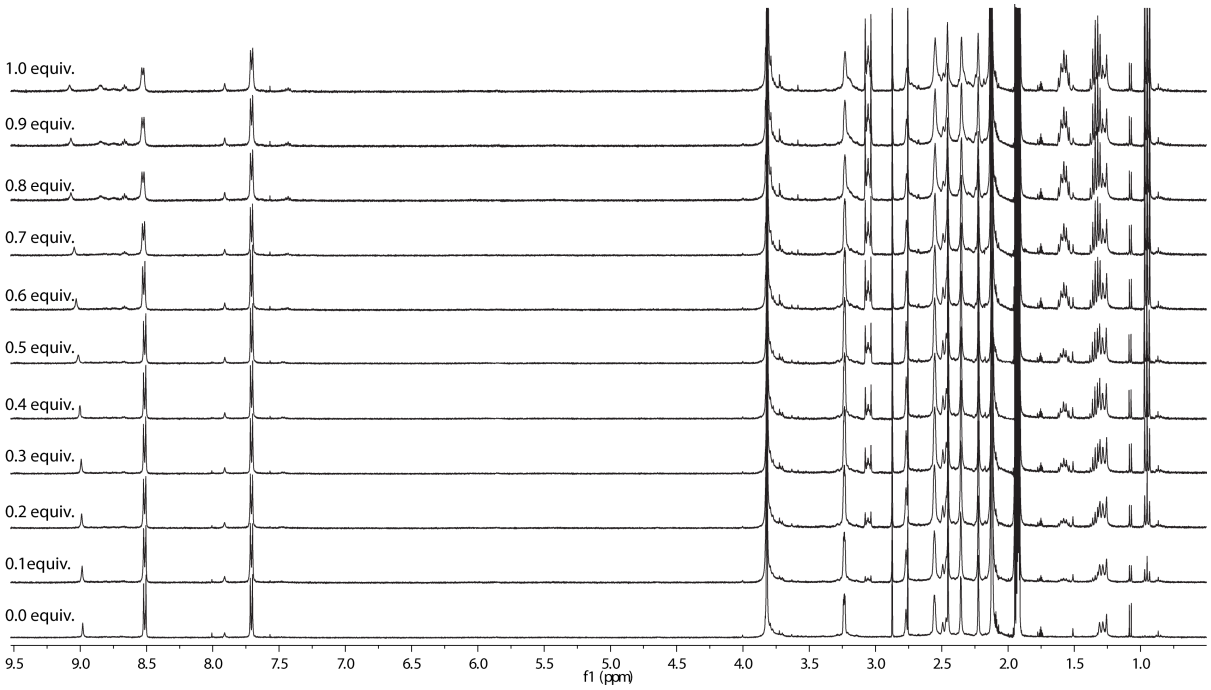

Figure S6 ^{1}H NMR titration (400 MHz, 298 K, CD_3CN) of $\{Pd_2\mathbf{L}_4\}$ with $(Bu_4N)_2[SiF_6]$.

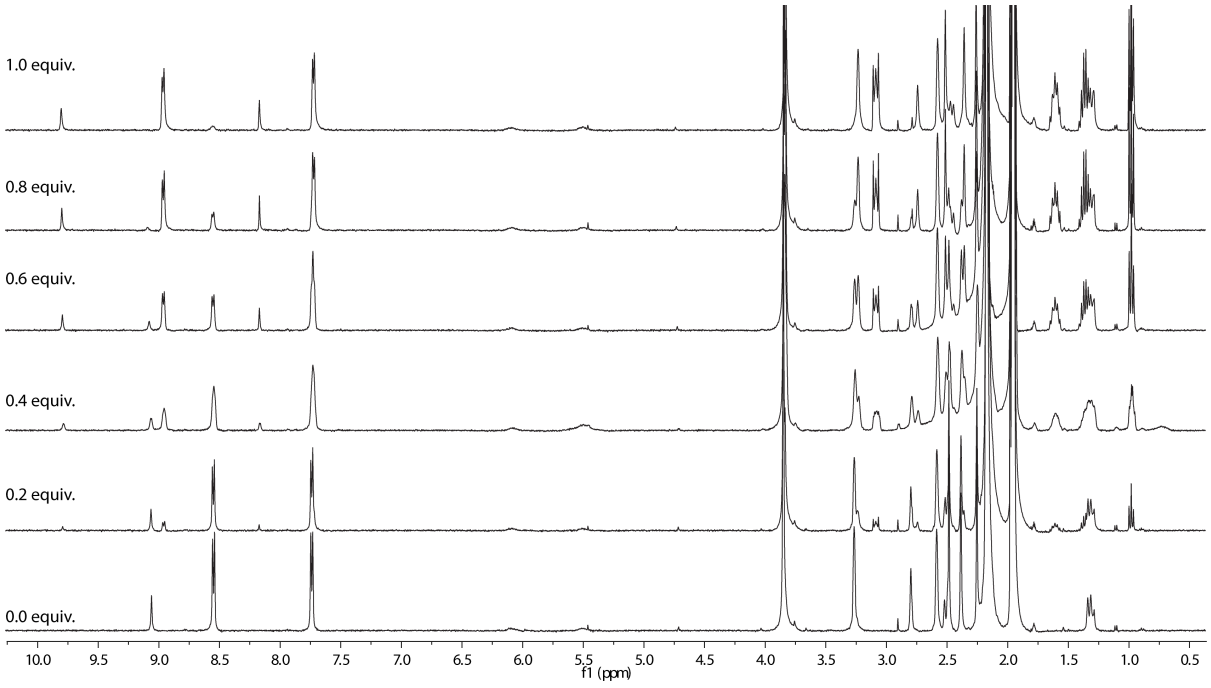

Figure S7 ^{1}H NMR titration (400 MHz, 298 K, CD_3CN) of $\{Pd_2\mathbf{L}_4\}$ with $(Bu_4N)_2$(benzene-1,4-disulfonate).

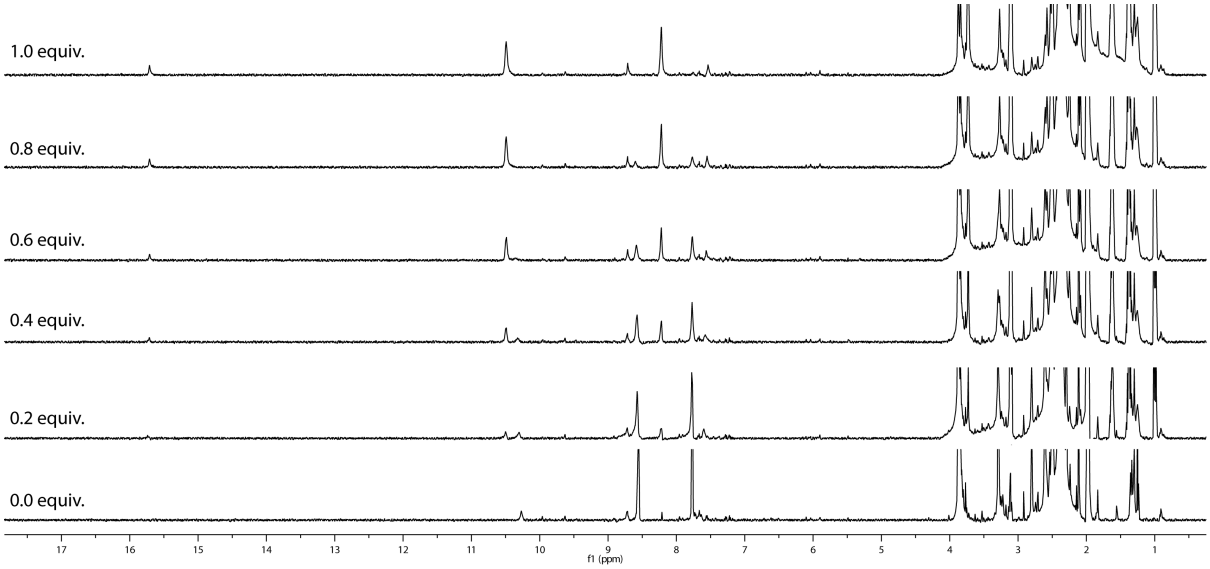

Figure S8 ^{1}H NMR titration (400 MHz, 298 K, CD_3CN) of $\{Pd_2\mathbf{L}_4\}$ with $(Bu_4N)_3[Fe(CN)_6]$.

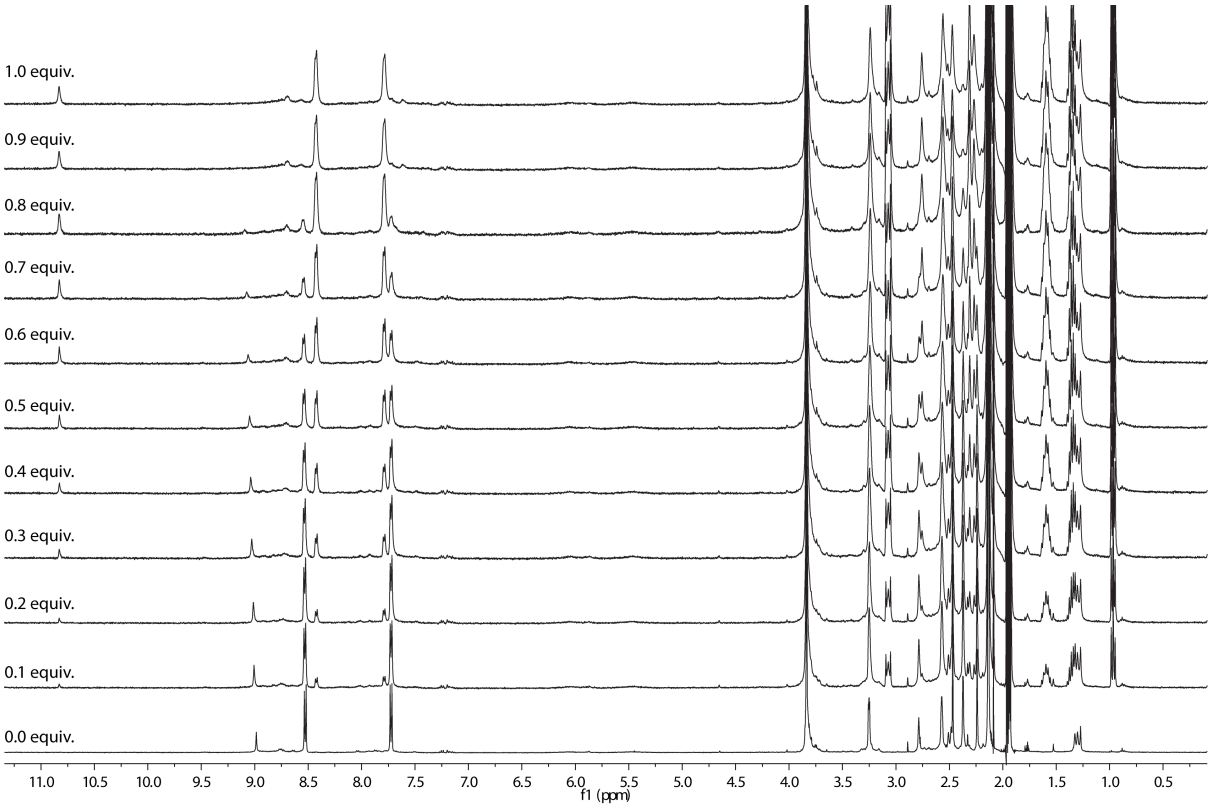

Figure S9 ^{1}H NMR titration (400 MHz, 298 K, CD_3CN) of $\{Pd_2\mathbf{L}_4\}$ with $(Bu_4N)_2[Pt(CN)_4]$.

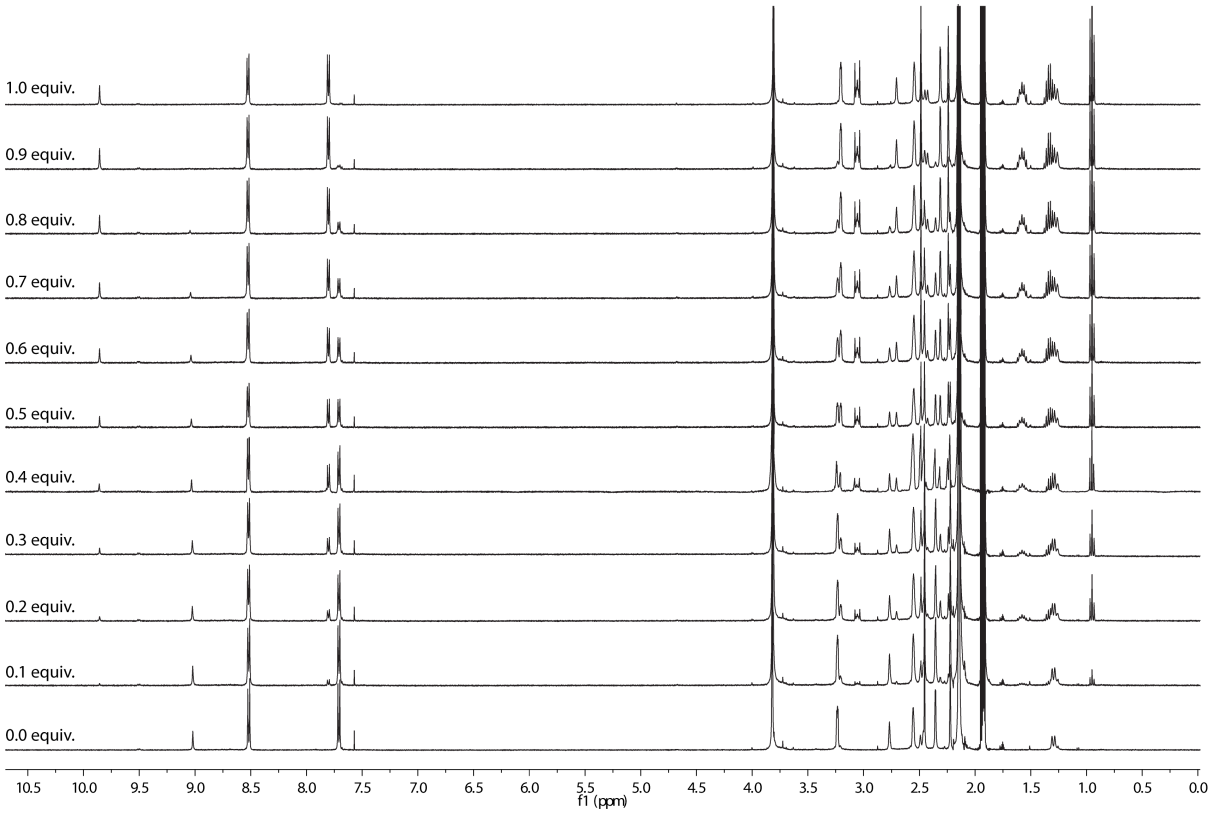

Figure S10 ^{1}H NMR titration (400 MHz, 298 K, CD_3CN) of $\{Pd_2\mathbf{L}_4\}$ with $(Bu_4N)_2[Pt(CN)_6]$.

ESI Mass Spectrometry, ^{13}C, ^{195}Pt and ^{1}H DOSY NMR Spectroscopy

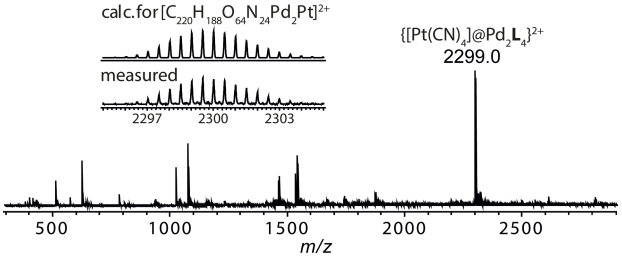

Figure S11 ESI-MS spectrum of $\{Pd_2\mathbf{L}_4\}$ + $(Bu_4N)_2[Pt(CN)_4]$.

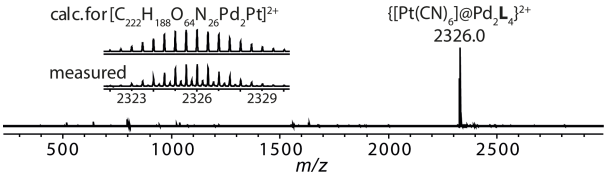

Figure S12 ESI-MS spectrum of $\{Pd_2\mathbf{L}_4\}$ + $(Bu_4N)_2[Pt(CN)_6]$.

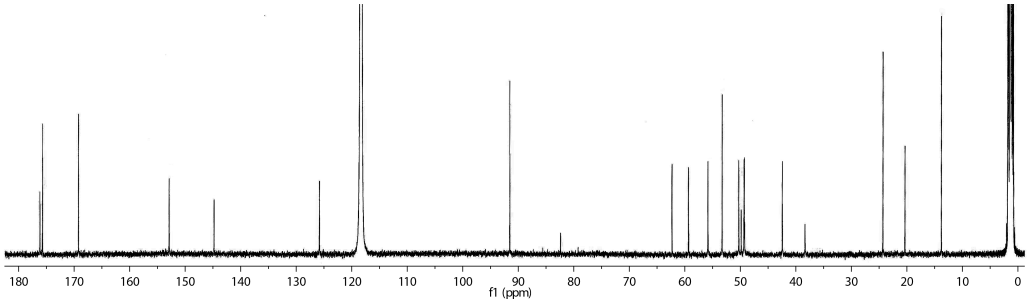

Figure S13 ^{13}C NMR spectrum of $\{[Pt(CN)_6]@Pd_2\mathbf{L}_4\}$.

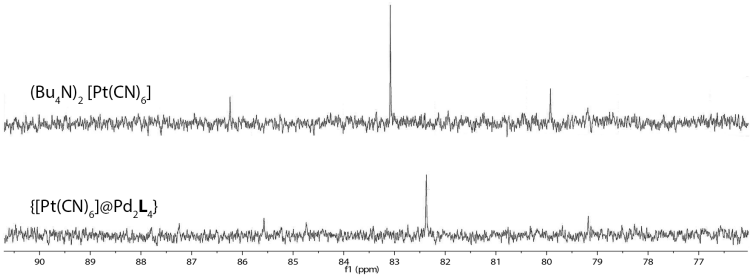

Figure S14 Expansion of ^{13}C NMR spectrum showing the nitrile carbon of a) $(Bu_4N)_2[Pt(CN)_6]$ and b) $\{[Pt(CN)_6]@Pd_2\mathbf{L}_4\}$.

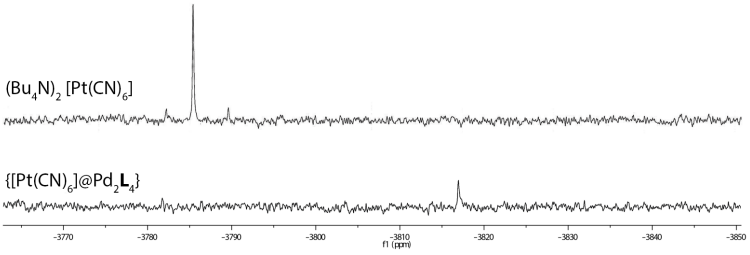

Figure S15 ^{195}Pt NMR spectrum of the free and encapsulated $[Pt(CN)_6]^{2-}$.

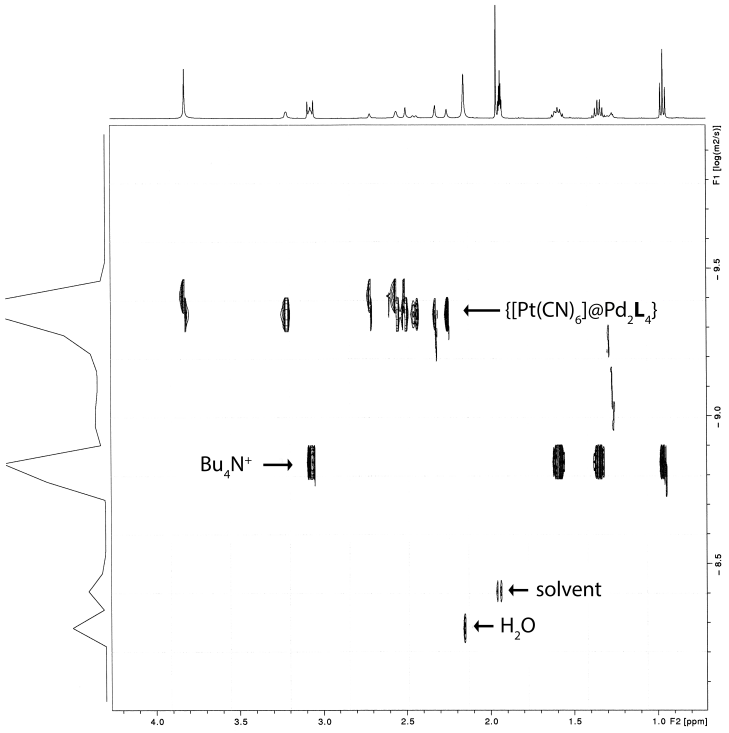

Figure S16 ^{1}H DOSY NMR spectrum of {[Pt(CN)$_6$]@Pd$_2$**L**$_4$} host-guest complex.

^{1}H NMR Titration Curve Fitting

Fitting of the NMR titration data (1:1 binding model) and calculation of the association constants were performed using a non-linear regression method with the Bindfit app.[7]

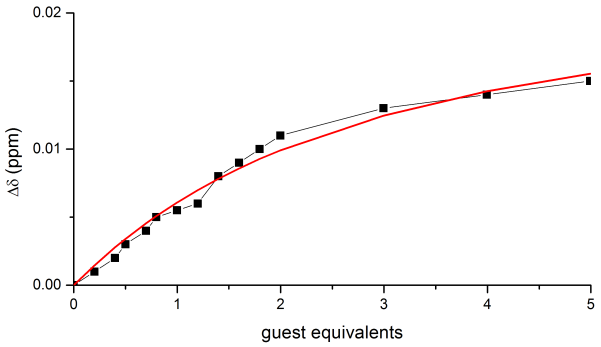

Figure S17 [Cr(CO)$_6$] titration, K = 596 M^{-1} (error = 8%).

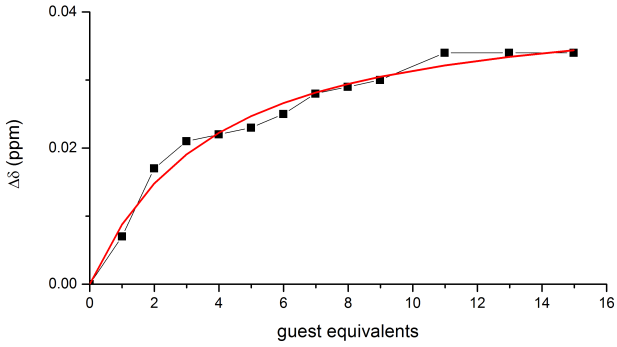

Figure S18 [Mo(CO)$_6$] titration, K = 395 M^{-1} (error = 8%).

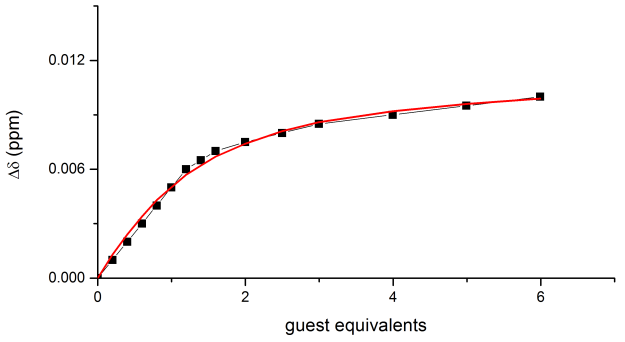

Figure S19 [W(CO)$_6$] titration, K = 1413 M^{-1} (error = 8%).

Single-Crystal X-Ray Diffraction

Single crystals suitable for X-ray crystallography were obtained by the slow diffusion of acetone into an acetonitrile solution of the host-guest complex. Due to the weak diffraction of the sample synchrotron radiation was required in order to achieve a reasonable resolution. Data were collected at the Macromolecular Crystallography Beamline X10SA of the Swiss Light Source employing silicon double crystal monochromated synchrotron radiation (0.9998 Å) with a single φ scan at 100(2) K. Data integration and reduction were undertaken with XDS[8] and XPREP[9]. Multi-scan empirical absorption correction was applied to the data using SADABS[10]. The structure was solved by intrinsic phasing/direct methods using SHELXT[11] and refined with SHELXL[12] using full-matrix least-squares routines on F^2 and ShelXle[13] as graphical user interface.

To facilitate structure refinement and molecular model building, a series of macromolecular refinement techniques has been carefully adapted and employed. These methods already proved successful in previous cases of huge and complicated supramolecular structures with high solvent content.[14] EXO ligands were grouped into residues to enable addressing all the atoms of repeating structural fragments with a single command. Stereochemical restraint dictionaries were generated using GRADE. GRADE is part of BUSTER[15] and was accessed via the GRADE Web Server.[16] Its dictionaries for SHELXL contain target values and standard deviations for 1,2-distances (DFIX) and 1,3-distances (DANG), as well as restraints for planar groups (FLAT). For the $[Pt(CN)_6]^{2-}$ guest similarity of bond length was defined (SADI) for the axial Pt-C bonds, axial C≡N bonds, equatorial Pt-C bonds and equatorial C≡N bonds, but no values of typical octahedral bonding environment (see table S3) were given as target as these would impose an octahedral bonding geometry and bias the observed values. The refinement of ADPs for all non-hydrogen and non-metal atoms was enabled by employing similarity (SIMU), isotropic restraints (ISOR) and enhanced rigid bond restraints (RIGU)[17] in the SHELXL program. Carbon-bound and nitrogen bound hydrogen atoms were included in idealized positions and refined using a riding model. The contribution of the electron density associated with disordered counterions and solvent molecules, which could not be modelled with discrete atomic positions were handled using the SQUEEZE[18] routine in PLATON[19]. Solvent masks (.fab files) generated by PLATON were included in the SHELXL refinement via the ABIN instruction in order to leave the original structure factors untouched.

Crystallographic data including structure factors have been deposited with CCDC 1447143. Copies of the data can be obtained free of charge at the CCDC website http://www.ccdc.cam.ac.uk/structures.

Crystallographic Data

Table S1 Crystallographic data for $\{[Pt(CN)_6]@Pd_2\mathbf{L}_4\}^{2+}$ structure

Structure, CCDC no.	$\{[Pt(CN)_6]@Pd_2\mathbf{L}_4\}^{2+}$, 1447143
Empirical formula	$C_{267}H_{278}Cl_2N_{26}O_{83}Pd_2Pt$
Mol. Weight / g mol^{-1}	5657.93
Temperature / *K*	100(2)
Wavelength / Å	0.9998
Crystal system	Monoclinic
Space group	C2/c
a / Å	41.03(10)
b / Å	23.27(8)
c / Å	39.83(12)
α / °	90
β / °	109.64(13)
γ / °	90
Volume / $Å^3$	35813(192)
Z	4
Density / g cm^{-3}	1.049
Absorption Coeff. / mm^{-1}	1.009
Crystal size / mm^3	0.250 x 0.210 x 0.180
θ range / °	5.730 to 25.813
Index ranges	-35 ≤ h ≤ 35 -20 ≤ k ≤ 20 -34 ≤ l ≤ 34
Reflections collected	156205
Independent reflections	12147 [R(int) = 0.1755]
Completeness	97.9 % (to theta = 25.813°)
Absorption correction	Empirical
Max. & min. transmission	0.7453 and 0.6012
Data / restraints / param.	12147 / 3740 / 1741
Goodness-of-fit on F^2	1.703
Final *R* indices [I > 2 s (I)]	R1 = 0.1429, wR2 = 0.4090
R indices (all data)	R1 = 0.1811, wR2 = 0.4392
Extinction coefficient	-
Larg. diff. peak/hole / e$Å^{-3}$	1.573 and -0.637
Flack x (Parsons)	-

Hydrogen Bond Table

Table S2 Hydrogen bonds for $\{[Pt(CN)_6]@Pd_2\mathbf{L}_4\}^{2+}$ structure

D-H...A	d(D-H) [Å]	d(H···A) [Å]	d(D···A) [Å]	<(DHA) [°]
N41_2-H41_2···N3_1	0.88	2.01	2.88(2)	176.3
N41_3-H41_3···N5_1	0.88	2.14	3.01(2)	178.2

Geometry of Encapsulated $[Pt(CN)_6]^{2-}$

The geometric analysis of the guest was complicated by the flexibility of the CN ligand positions which are reflected in large atomic displacement parameters and resulted in severe librational shortening effects of the Pt-C bonds. These systematic shortenings are a well-known artefact.[20] The situation is illustrated in Figure **S20**.

Although being much shorter than values found in the literature (see Table **S3** and **S4**), the axial and equatorial positions of the CN ligands were found to deviate from each other significantly. While Pt-C bonds were found to be shorter in axial positions than in equatorial positions, it is vice versa with CN bonds.

Due to the high flexibility and resulting librational shortening effect, the X-ray data cannot provide conclusive evidence for the tetragonal distortion of the $[Pt(CN)_6]^{2-}$ complex on its own, but provides a sensible explanation for the IR signal splitting. The combination of both observations led us propose a tetragonal distortion of the guest inside the supramolecular host.

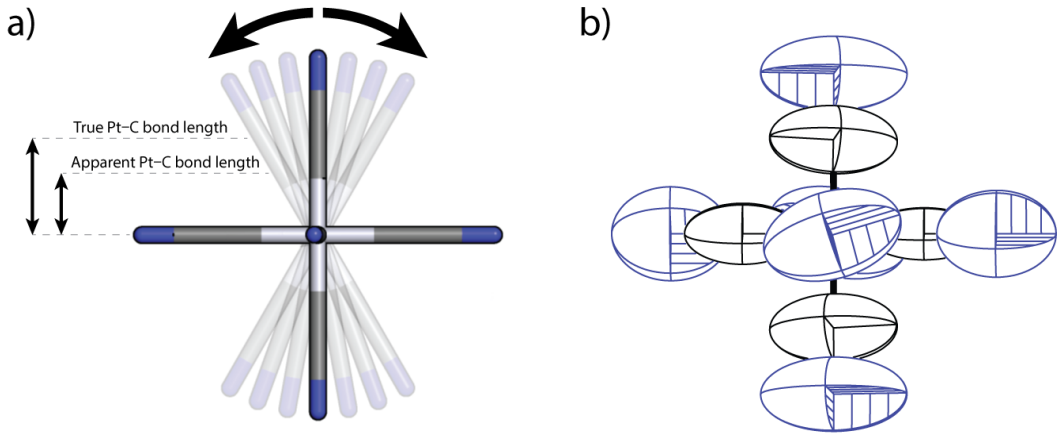

Figure S20 a) Schematic showing librational shortening[20] of Pt–C bond lengths by minor disorder of movement of the bound guest, b) ORTEP of encapsulated $[Pt(CN)_6]^{2-}$ represented as 90% probability ellipsoids.

Table S3 Bonds length for encapsulated $[Pt(CN)_6]^{2-}$

Bond length	Å
axial	
Pt1_1-C6_1	1.53(4)
Pt1_1-C8_1	1.55(4)
N9_1-C8_1	1.36(3)
C6_1-N7_1	1.35(3)
equatorial	
Pt1_1-C4_1	1.73(2)
Pt1_1-C2_1	1.805(18)
C2_1-N3_1	1.271(19)
C4_1-N5_1	1.254(19)

Table S4 Bonds length of octahedral $[Pt(CN)_6]^{2-}$ from literature[21] (CCDC: YASNUC)

Bond length	Å
Pt-C(6)	2.015(3)
Pt-C(4)	2.016(3)
Pt-C(1)	2.022(3)
Pt-C(3)	2.022(3)
Pt-C(2)	2.023(3)
Pt-C(5)	2.026(3)
N(1)-C(1)	1.131(4)
N(2)-C(2)	1.132(4)
N(3)-C(3)	1.136(4)
N(4)-C(4)	1.131(4)
N(5)-C(5)	1.132(4)
N(6)-C(6)	1.134(4)

References

[1] G. P. Moss, *Pure Appl. Chem.* **1999**, *71*, 513–529.

[2] T. Rohmer, C. Lang, C. Bongards, K. B. S. S. Gupta, J. Neugebauer, J. Hughes, W. Gärtner, J. Matysik, *J. Am. Chem. Soc.,* **2010**, *132*, 4431–4437.

[3] M. Golic, M. R. Johnston, D. Margetić, A. C. Schultz, R. N. Warrener, *Aust. J. Chem,* **2006**, *59*, 899–914.

[4] M. G. Banwell, N. L. Hungerford, K. A. Jolliffe, *Org. Lett.,* **2004**, *6*, 2737–2740.

[5] M. a. D. Duque, C. Ma, E. Torres, J. Wang, L. Naesens, J. Juárez-Jiménez, P. Camps, F. J. Luque, W. F. DeGrado, R. A. Lamb, L. H. Pinto, S. Vázquez, *J. Med. Chem.,* **2011**, *54*, 2646–2657.

[6] Gaussian '09, Revision A.02, M. J. Frisch, G. W. Trucks, H. B. Schlegel, G. E. Scuseria, M. A. Robb, J. R. Cheeseman, G. Scalmani, V. Barone, B. Mennucci, G. A. Petersson, H. Nakatsuji, M. Caricato, X. Li, H. P. Hratchian, A. F. Izmaylov, J. Bloino, G. Zheng, J. L. Sonnenberg, M. Hada, M. Ehara, K. Toyota, R. Fukuda, J. Hasegawa, M. Ishida, T. Nakajima, Y. Honda, O. Kitao, H. Nakai, T. Vreven, J. Montgomery, J. A., J. E. Peralta, F. Ogliaro, M. Bearpark, J. J. Heyd, E. Brothers, K. N. Kudin, V. N. Staroverov, R. Kobayashi, J. Normand, K. Raghavachari, A. Rendell, J. C. Burant, S. S. Iyengar, J. Tomasi, M. Cossi, N. Rega, J. M. Millam, M. Klene, J. E. Knox, J. B. Cross, V. Bakken, C. Adamo, J. Jaramillo, R. Gomperts, R. E. Stratmann, O. Yazyev, A. J. Austin, R. Cammi, C. Pomelli, J. W. Ochterski, R. L. Martin, K. Morokuma, V. G. Zakrzewski, G. A. Voth, P. Salvador, J. J. Dannenberg, S. Dapprich, A. D. Daniels, Ö. Farkas, J. B. Foresman, J. V. Ortiz, J. Cioslowski, D. J. Fox, Gaussian, Inc., Wallingford CT, **2009**.

[7] a) P. Thordarson, *Chem. Soc. Rev*., **2011**, 40, 1305–1323; b) http://www.supramolecular.org

[8] W. Kabsch, Acta Cryst. D, 2010, 66, 125–132.

[9] Bruker-Nonius, APEX, SAINT, SADABS and XPREP, Bruker AXS Inc., Madison, Wisconsin, USA, 2013.

[10] G. M. Sheldrick, Acta Cryst. A, 2015, 71, 3−8.

[11] G. M. Sheldrick, Acta Cryst. C, 2015, 71, 3−8.

[12] C. B. Hübschle, G. M. Sheldrick and B. Dittrich, J. Appl. Cryst., 2011, 44, 1281–1284.

[13] a) M. Pascu, M. Marmier, C. Schouwey, R. Scopelliti, J. J. Holstein, G. Bricogne and K. Severin, Chem. Eur. J., 2014, 20, 5592–5600. b) C. Schouwey, J. J. Holstein, R. Scopelliti, K. O. Zhurov, K. O. Nagornov, Y. O. Tsybin, O. S. Smart, G. Bricogne and K. Severin, Angew. Chem., Int. Ed., 2014, c) T. K. Ronson, C. Giri, N. K. Beyeh, A. Minkkinen, F. Topić, J. J. Holstein, K. Rissanen and J. R. Nitschke, Chem. Eur. J. 2013, 19, 3374–3382.

[14] G. Bricogne, E. Blanc, M. Brandl, C. Flensburg, P. Keller, P. Paciorek, P. Roversi, A. Sharff, O. Smart, C. Vonrhein and T. Womack, BUSTER version 2.13.0, 2011, Global Phasing Ltd., Cambridge, United Kingdom.

[15] http://grade.globalphasing.org

[16] A. Thorn, B. Dittrich and G. M. Sheldrick, Acta Cryst. A, 2012, 68, 448–451.

[17] D. Kratzert, J. J. Holstein and I. Krossing, J. Appl. Cryst. 2015, 48, 933−938, https://www.xs3.uni-freiburg.de/research/dsr

[18] P. van der Sluis and A. L. Spek, Acta Cryst. A, 1990, 46, 194–201.

[19] A. L. Spek, PLATON: A Multipurpose Crystallographic Tool, 2008, Utrecht University, Utrecht, The Netherlands.

[20] Steed, J. W.; Atwood, J. L., *Supramolecular Chemistry*. 2nd Ed.; Wiley-VCH: Chichester, UK, 2009, p449.

[21] J. A Schlueter, R. J. Funk, U. Geiser, Acta Cryst. C, 2005, 61, m304 – m306.